Int. J. Multiphase Flow Vol. 8, No. 5, pp. 525–542, 1982
Printed in Great Britain.

0301-9322/82/050525-18$03.00/0
Pergamon/Elsevier

ON THE CALCULATION OF WALL TEMPERATURES IN THE POST DRYOUT HEAT TRANSFER REGION

R. A. MOOSE† and E. N. GANIĆ‡

Department of Energy Engineering, University of Illinois, Chicago, IL 60680, U.S.A.

(*Received* 26 *May* 1981; *in revised form* 2 *February* 1982)

Abstract—A non-equilibrium post dryout heat transfer model for calculating the wall temperature distribution in vertical upflows is presented in this study. The model is based upon the three path heat transfer formulation developed by MIT researchers (Laverty & Rohsenow 1964, Forslund & Rohsenow 1968, Hynek *et al.* 1969 and Plummer *et al.* 1974) that involves heat transfer from wall to vapor, from wall to droplets in contact with the wall and from vapor to liquid droplets in the vapor core. Downstream gradients for the bulk vapor temperature, vapor quality, droplet size and vapor velocities are identical to those used by Hynek *et al.* (1969) and Plummer *et al.* (1974). Conditions at the dryout location are calculated using a modified version of a technique developed by Hynek *et al.* (1969).

A procedure for determining an average droplet diameter based on a size distribution is introduced. Migration of droplets through the boundary layer and droplet deposition flux are predicted with the model of Ganić & Rohsenow (1979). Heat transfer from the wall to the impinging liquid droplets is calculated with a correlation by Holman & McGinnis (1969). Mechanisms contributing to wall to droplet heat transfer are identified as (a) droplet-wall contact, (b) intensive droplet evaporation inside the boundary layer, and (c) destruction of the boundary layer due to droplet migration to, and rebound from, the hot surface. The significance of the average droplet size and size distribution is demonstrated through its control over the free stream evaporation and droplet deposition rates.

Predicted uniform heat flux wall temperature profiles for water, nitrogen and freon 12 are in good agreement with the data of Era *et al.* (1966), Bennett *et al.* (1967), Forslund & Rohsenow (1968), Ling *et al.* (1971), Groeneveld (1972) and Janssen & Kervinen (1975).

1. INTRODUCTION

Post dryout heat transfer is of ever increasing importance particularly in the design of steam generators, nuclear reactor cooling systems, spray coolers, cryogenic equipment, quenching processes in metallurgy and other industrial applications. Various workers over the past two decades attempted to explain post dryout heat transfer through identification of individual mechanisms. Laverty & Rohsenow (1964) began with a two step model that included vapor superheating at the wall and vapor cooling due to liquid evaporation in the free stream. The liquid phase was represented by a homogenous mixture of spherical droplets. Forslund & Rohsenow (1968) extended this model by including the direct wall to droplet heat transfer, a droplet splitting mechanism and an improved drag coefficient. Hynek *et al.* (1969) proposed further modifications consisting primarily of a new procedure for calculating initial liquid and vapor velocities. Plummer *et al.* (1974) then replaced the direct wall to liquid heat transfer correlation based on Leidenfrost phenomena with a heat conduction term assuming a linear temperature profile through the boundary layer. Ganić & Rohsenow (1976) proposed an independent model for calculating the heat transfer from the wall to the dispersed flow which focused on the structure and dynamics of the liquid phase. The liquid phase was represented by a characteristic droplet size based upon a size distribution and most probable size. Equations of motion for droplets traversing the boundary layer were solved to determine mass deposition and direct wall to droplet heat transfer rates.

A model similar to the Forslund–Rohsenow model was independently developed by Bennett *et al.* (1967). Styrikovich *et al.* (1977, 1980) emphasized the role of artificial roughness in the enhancement of heat transfer at the wall.

Various parametric studies by Nijhawan *et al.* (1980), Nelson (1980), Yarkho *et al.* (1977), Yao & Rane (1980), and Michiyoshi & Makino (1979) have indicated that the degree of non-equilibrium and heat transfer characteristics of the liquid droplets play major roles in

†Research Assistant, presently with Sonicraft, Inc., Chicago, Illinois, U.S.A.
‡Present address: University of Sarajevo, Faculty of Mechanical Engineering, Post.fah 107, 71000-Sarajevo, Yugoslavia.

determining overall heat transfer rates and subsequent wall temperatures. Chen *et al.* (1977) proposed a model that included a detailed representation of individual boiling mechanisms occurring at the hot wall. Extensive literature surveys by Chen *et al.* (1977), Mayinger & Langner (1978) and Bennett *et al.* (1967), provide a complete summary of the work done in the field of post dryout heat transfer.

The present work follows the model of Hynek *et al.* (1969), but replaces the homogeneous spherical droplet liquid phase and Leidenforst heat transfer correlation with the more complete development of Ganić & Rohsenow (1976). Further refinements include more recent correlations for the droplet size distribution by Cumo *et al.* (1973) and for the wall to impinging droplet heat transfer rates by Holman & McGinnis (1969). Accurate representation of the liquid phase is emphasized since droplet size and motion controls the rate of evaporation in the free stream, the rate of deposition onto the heated wall and the efficiency of evaporation upon impact. Throughout the course of this work the effect and significance of each modification is discussed, emphasizing the coupling of the physical mechanisms involved.

2. STRUCTURE AND DYNAMICS OF DISPERSED FLOW

Dispersed flow regimes are likely to result if CHF occurs at high vapor fractions. The liquid droplets formed usually assume a spherical shape due to surface tension. Cumo *et al.* (1973) performed extensive experimental research on droplet sizes in highly dispersed two phase turbulent flows using freon 12 as the test fluid. Similar studies were done by Tatterson *et al.* (1977) and Azzopardi *et al.* (1978). Based on their results the following conclusions can be drawn:

(a) Two phase highly dispersed turbulent flows are characterized by a statistically uniform spatial distribution of the entrained droplets, independent of their size and the local vapor velocity.

(b) The droplets follow a size distribution which is parameterized by a most probable droplet size.

(c) The droplet size distribution becomes more uniform as the number of droplets increases.

The information given above is sufficient to characterize the structure of highly dispersed two phase mixtures.

2.1 *Droplet size distribution*

Droplet size distribution by Cumo *et al.* (1973), Tatterson *et al.* (1977), and Azzopardi *et al.* (1978) have been presented in the literature. The following distribution suggested by Cumo *et al.* (1973) has been chosen for use in the present model:

$$n(D) = \frac{D}{D_*^2} \exp\left(\frac{-D}{D_*}\right) \qquad [1]$$

where,

$$\int_{D_1}^{D_2} n(D)\,\mathrm{d}D = P(D) \qquad [2]$$

and $P(D)$ is the probability that the diameter, D lies between D_1 and D_2, subscript $*$ is for most probable. This distribution is normalized such that:

$$\int_0^\infty n(D)\,\mathrm{d}D = 1. \qquad [3]$$

2.2 *Most probable droplet size*

The flow regime present when CHF occurs at high vapor fractions is annular, resulting in liquid droplet entrainment in the high velocity vapor. The correlations of Tatterson *et al.* (1977),

and Azzopardi *et al.* (1978) based on stripping mechanism experiments were considered for use in the heat transfer model. The correlation of Tatterson *et al.* (1977) for air–water systems showed reasonable agreement with the size data of several other researchers (Cumo *et al.* 1973, Azzopardi *et al.* 1978, Nukiyama & Tanasawa 1939, Boll *et al.* 1974, James 1976, and Hinze 1949) and resulted in the best prediction of wall temperature data when the most probable diameter D_*, was taken to be the mass median diameter D_{mm}:

$$D_* \simeq D_{mm} = 0.016 \left(\frac{\rho_G V_G^2 d f_s}{2\sigma} \right)^{-0.5} d \qquad [4]$$

where f_s is the smooth wall fraction factor assumed to be $0.046\,\mathrm{Re}^{-0.20}$, ρ_G is the saturated vapor density, d is the tube diameter, f_s is the smooth wall friction factor, σ is the surface tension, subscript *mm* is mass medium.

2.3 *Maximum droplet size*

To suitably define mean characteristic droplet sizes based on the droplet size distribution of [1] it is necessary to know the maximum possible droplet size. The Weber number is the most important dimensionless group for determining the stability of a drop. If the Weber number,

$$\mathrm{We} = \frac{\rho_G (V_G - V_L)^2 D}{\sigma}, \qquad [5]$$

where V_G is the saturated vapor velocity and V_L is the liquid velocity, exceeds a critical value, droplets shatter into several small droplets, each having a lower Weber number. Critical Weber numbers have been measured experimentally by Isshiki (1959) and Forslund & Rohsenow (1966) who found We_c to equal 6.5 to 7.5 respectively. Therefore, the maximum droplet size can be determined as:

$$D_{\max} = \frac{\mathrm{We}_c \sigma}{\rho_G (V_G - V_L)^2} \qquad [6]$$

Upon calculation of $D_{\max}$ for the experimental conditions used for comparison with the heat transfer model, $D_{\max}$ was found to be approximately two orders of magnitude larger than D_*. The probability of such a size as given by [1] is approximately zero. This simplifies the development of the relationships to follow by allowing the upper limits of integration to be changed from $D_{\max}$ to infinity.

2.4 *Characteristic mean droplet size*

Characteristic mean droplet sizes are often defined in an attempt to accurately represent an entire droplet size distribution by a single size. Depending on the physical phenomena being considered, the definitions can vary, although all take the form,

$$D_{mn} = \left[\frac{\int_0^{D_{\max}} D^m n(D)\,\mathrm{d}D}{\int_0^{D_{\max}} D^n n(D)\,\mathrm{d}D} \right]^{1/(m-n)} \qquad [7]$$

where m, n are drop size indices, $D_{\max}$ is the maximum droplet diameter, $n(D)$ is defined by [1] and [4]. By letting $D_{\max}$ go to infinity, and recognizing the integrals as Γ-functions, the following result is readily obtained:

$$D_{mn} = \left[\frac{\Gamma(m+2) D_*^{m+1}}{\Gamma(n+2) D_*^{n+1}} \right]^{1/(m-n)} = \left[\frac{(m+1)! D_*^{m-n}}{(n+1)!} \right]^{1/(m-n)}, \qquad [8]$$

where Γ is the gamma function.

Since both droplet surface area and droplet mass are important for calculating slip ratios (V_G/V_L), heat transfer from vapor to droplet, and heat transfer from wall to droplet, the Sauter mean diameter D_{32} was chosen as the characteristic droplet size. With $m = 3$ and $n = 2$, [8] reduces to

$$D_{32} = 4D_*. \quad [9]$$

The Sauter mean diameter as given by [9] results in droplet sizes on the order of 200 to 300 μm.

2.5 *Migration of droplets through the boundary layer*

A theoretical analysis of droplet deposition from a vapor stream to a heated wall has been performed by Ganić & Rohensow (1976). Equations of motion for a droplet moving through the boundary layer in a vertical upflow along with the necessary boundary and initial conditions can be found in their study.

A numerical routine has been modified (Shampine *et al.* 1976, Moose 1980) to solve the differential equations of motion iteratively by binary search to determine the diameter of the smallest droplet deposited on the heated wall for a given set of conditions (V_G, V_L, T_w, V_0). This is the deposition cutoff diameter D_c. Droplets smaller than D_c are returned to the vapor stream, while droplets larger than D_c strike the heated wall. For a known value of the deposition diameter D_c, a cumulative mass deposition factor can be defined as:

$$f_c = \frac{\int_{D_c}^{D_{max}} D^3 n(D)\,dD}{\int_0^{D_{max}} D^3 n(D)\,dD} = \frac{1}{24}\exp\left[\bar{D}^4 + 4\bar{D}^3 + 12\bar{D}^2 + 24\bar{D} + 24\right] \quad [10]$$

where, the subscript c is for critical, and

$$\bar{D} = \frac{D_c}{D_*}. \quad [11]$$

This represents the fraction of the mass entering the boundary layer that impinges on the heated surface. Furthermore, the average droplet size striking the wall can be expressed as:

$$\bar{D}_{10} = \frac{\int_{D_c}^{D_{max}} Dn(D)\,dD}{\int_{D_c}^{D_{max}} n(D)\,dD} = \left[\frac{\bar{D}^2 + 2\bar{D} + 2}{\bar{D} + 1}\right] D_*. \quad [12]$$

Equations [10] and [12] are used extensively in the calculation of the amount of heat transferred directly from the heated wall to the impinging liquid droplets.

3. POST DRYOUT HEAT TRANSFER MODEL

3.1 *General properties of the model*

The model is applicable to high void dryout, vertical upflows and has the following major properties:

(a) The phases are assumed to be in thermodynamic equilibrium at the dryout point, as a result of the liquid film dryout.

(b) The vapor phase is assumed to be a continuum, and can become superheated downstream of the dryout location.

(c) The liquid phase is assumed to be in the form of spherical droplets, characterized statistically as discussed in section 2. The liquid remains at the saturation temperature throughout the calculation procedure.

(d) The heat transfer mechanisms identified are, wall to vapor, vapor to liquid, and wall to liquid.

(e) Thermophysical properties are temperature dependent, and are calculated with polynomial fits of experimental data.

(f) All calculations are performed using a modified version of a computer code by Hynek *et al.* (1969). Subroutines have been added to calculate properties and droplet deposition rate.

(g) The standard input parameters are heat flux, mass flux, dryout quality and tube diameter.

(h) The primary output of the program is the wall temperature profile at step by step axial locations.

3.2 *Dryout conditions*

Initial liquid and vapor velocities are calculated using a modified version of an iterative technique by Hynek *et al.* (1969) who solved the momentum and continuity equations along with assumptions relating initial liquid and vapor accelerations to the heat flux under isothermal conditions to give two independent equations relating $(V_G)_{DO}$ and $(V_L)_{DO}$. Once liquid and vapor velocities were known, Hynek *et al.* (1969) calculated a droplet diameter by assuming that $We = We_c = 7.5$. At downstream locations the Weber number was calculated, and if it exceeded the critical value of 7.5 droplets were assumed to split into two smaller droplets of equal size. The only change to Hynek's iteration scheme was the replacement of the expression for the Weber number,

$$We = We_c = 7.5 \qquad [13]$$

with

$$We = \frac{\rho_v (V_v - V_L)^2 D_{32}}{\sigma}. \qquad [14]$$

Thus the Weber number and dryout droplet size are also determined during the iteration for the liquid and vapor velocities. It was found that We was not equal to We_c at the dryout location as assumed by Hynek *et al.* (1969). In all cases studied in this paper (figures 1–16) We was much less than We_c and therefore no droplet break-up occurred.

3.3 *Gradients in post dryout*

The post dryout gradients of Hynek *et al.* (1969) which are identical to those used by other workers (Plummer *et al.* 1974, Bennett *et al.* 1967, and Groeneveld 1972) are used in the present model.

Droplet velocity gradient:

$$\frac{dV_L}{dZ} = \frac{3C_D \rho_v (V_G - V_L)^2}{4D_{32}\rho_L V_L} - \left[1 - \frac{\rho_v}{\rho_L}\right]\frac{g}{V_L} \qquad [15]$$

where C_D is the drag coefficient, the subscript 32 is for the Sauter mean, g is the gravitational calculation, Z is the length except for the first interval, where:

$$\frac{dV_L}{dZ} = \frac{4q_t X_e}{H_{LG}\, d\rho_G}. \qquad [16]$$

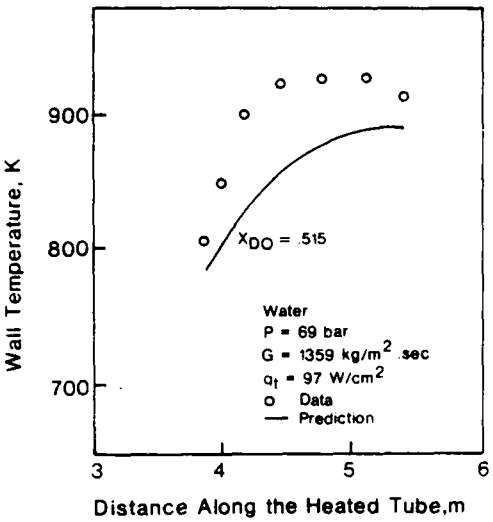

Fig. 1.

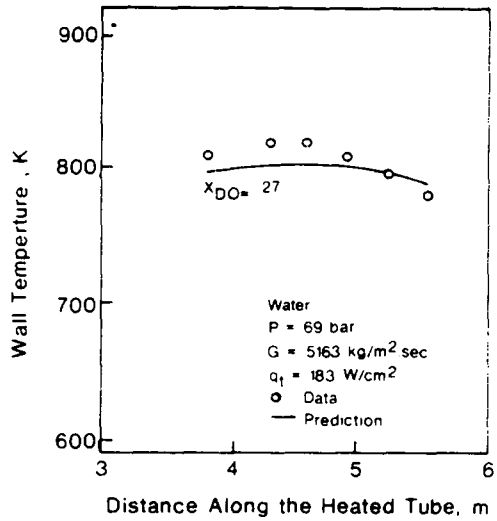

Fig. 2.

Figure 1. Comparison with Bennett's water data (Bennett *et al.* 1967).

Figure 2. Comparison with Bennett's water data (Bennett *et al.* 1967).

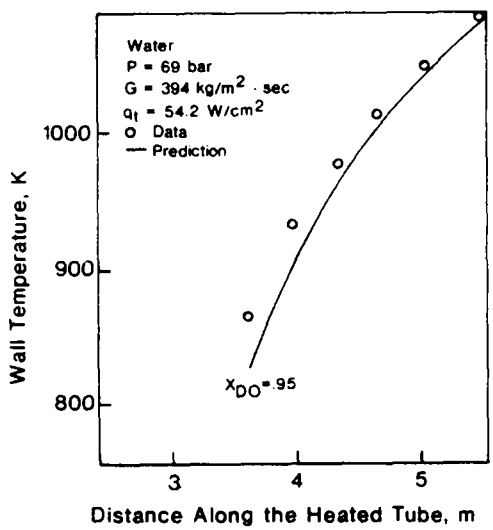

Fig. 3.

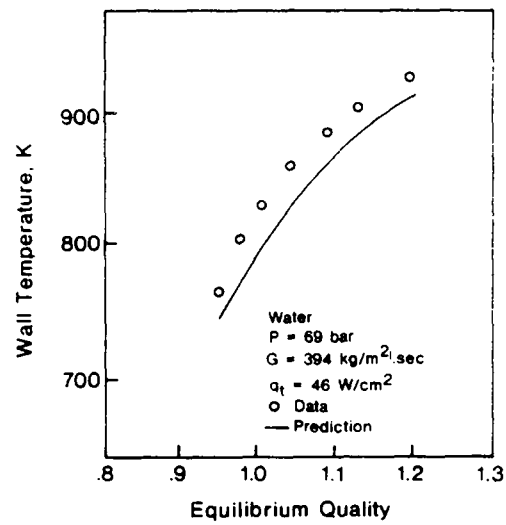

Fig. 4.

Figure 3. Comparison with Bennett's water data (Bennett *et al.* 1967).

Figure 4. Comparison with Bennett's water data (Bennett *et al.* 1967).

q_t is the total heat flux, H_{LG} is the specific latent heat of vaporization, X_a is the actual quality
Droplet diameter gradient:

$$\frac{dD_{32}}{dZ} = \frac{-2q_{wd}}{H_{LG}\rho_L V_L} - \frac{4D_{32}q_{wd}}{3(1-X_A)\,dGH_{LG}}. \quad [17]$$

Actual quality gradient:

$$\frac{dX_a}{dZ} = \frac{-3(1-X_{DO})D_{32}^2}{D_{DO}^3} \cdot \frac{dD_{32}}{dZ}. \quad [18]$$

Equilibrium quality gradient:

$$\frac{dX_e}{dZ} = \frac{4q_t}{GH_{LG}d}. \quad [19]$$

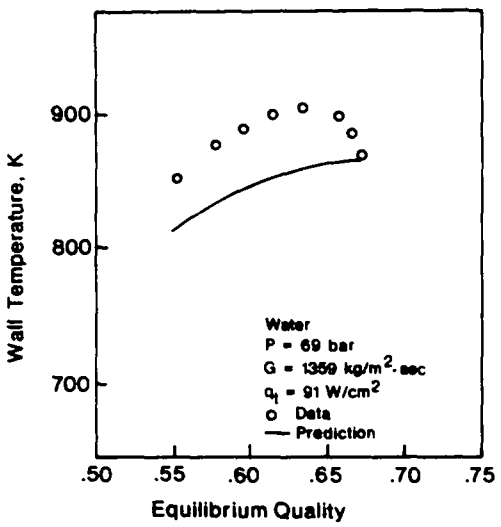

Fig. 5.

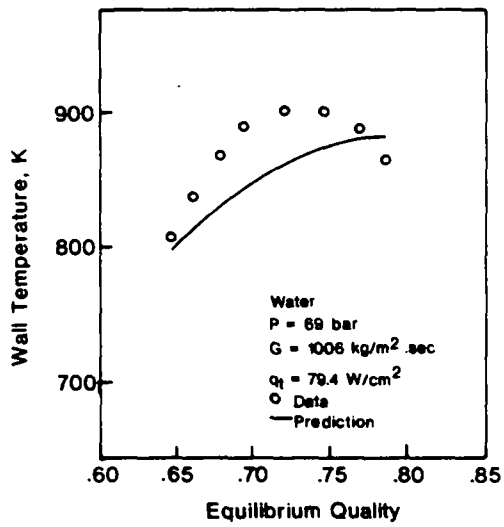

Fig. 6.

Figure 5. Comparison with Bennett's water data (Bennett *et al.* 1967).

Figure 6. Comparison with Bennett's water data (Bennett *et al.* 1967).

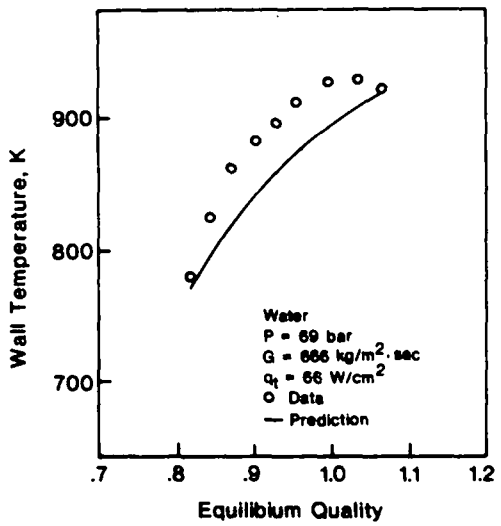

Fig. 7.

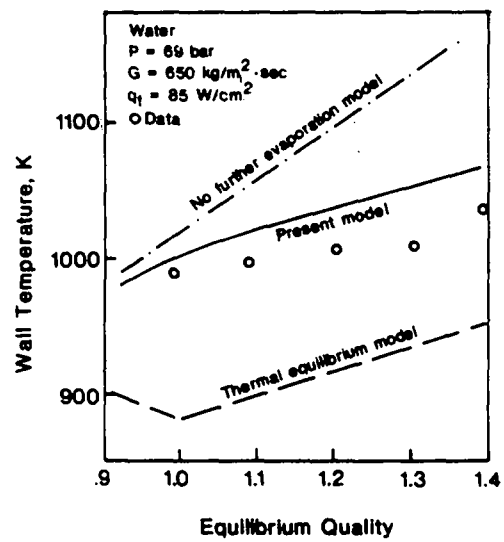

Fig. 8.

Figure 7. Comparison with Bennett's water data (Bennett *et al.* 1967).

Figure 8. Comparison with Bennett's water data (Bennett *et al.* 1967).

where X_e is the equilibrium quality, X_{DO} is the quality on dry out, q_{wd} is the wall to drop heat flux Vapor temperature gradient:

$$\frac{dT_v}{dZ} = \frac{H_{LG}\frac{dX_e}{dZ} - [H_{LG} + C_{pv}(T_v - T_s)]\frac{dX_A}{dZ}}{X_A C_{pv}}. \quad [20]$$

These gradients allow the calculation of the quantities at successive axial locations as:

$$F_{I+1} = F_I + \frac{dF}{dZ}dZ \quad [21]$$

where F is any quantity of interest.

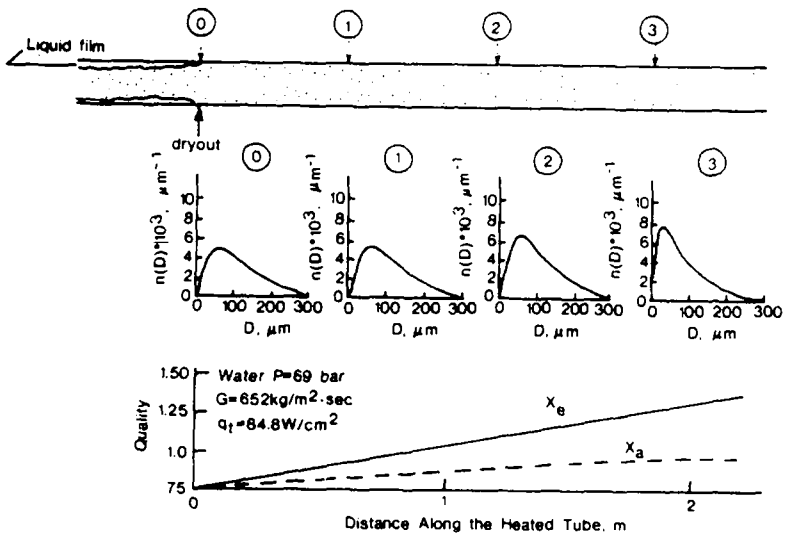

Figure 9. Variation of the droplet size distribution, actual quality and equilibrium quality along the uniformly heated tube.

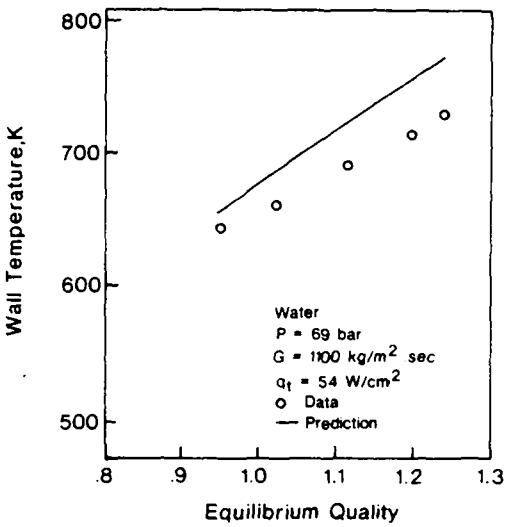

Fig. 10.

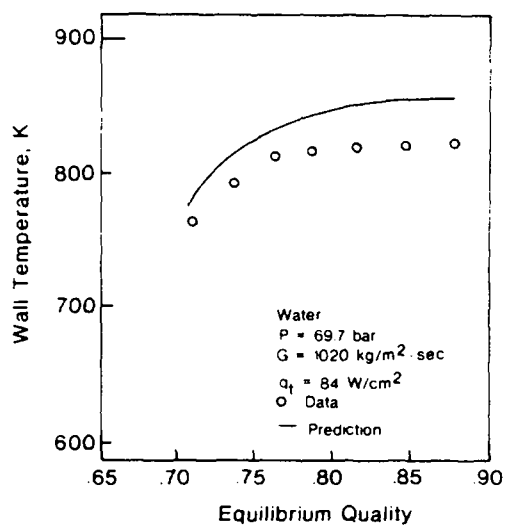

Fig. 11.

Figure 10. Comparison with Era's water data (Era *et al.* 1966).

Figure 11. Comparison with Janssen's and Kervinen's water data (Janssen & Kervinen 1975).

3.4 *Vapor to droplet heat transfer*

The following expression (Hynek *et al.* 1969) is used to calculate the amount of heat transferred to a single droplet in the vapor stream,

$$q_{vd} = \frac{2(T_v - T_s)k_v}{D_{32}}(1 + 0.276\,\mathrm{Re}_d^{0.5}\,\mathrm{Pr}_v^{0.33}). \qquad [22]$$

3.5 *Wall to vapor heat transfer*

Numerous single phase vapor heat transfer correlations exist in the literature. These correlations are all of similar form and are differentiated only by the experimental conditions on which they are based. The following temperature dependent correlation (McAdams 1954) is used in the present model.

$$h_{wv} = \frac{k_v}{d} \cdot (0.023\,\mathrm{Re}_v^{0.8}\,\mathrm{Pr}_v^{0.33})\left(\frac{\mu_v}{\mu_w}\right)^{0.14}. \qquad [23]$$

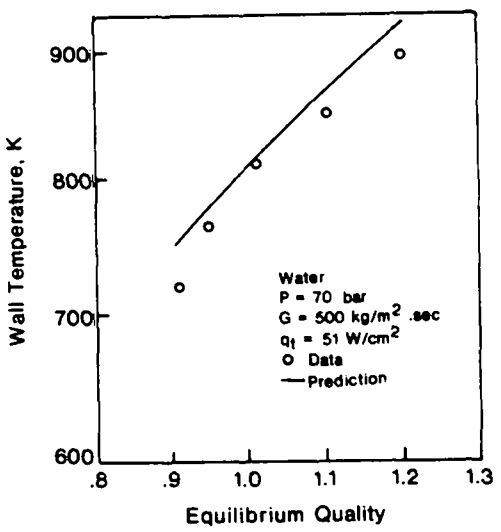

Fig. 12.

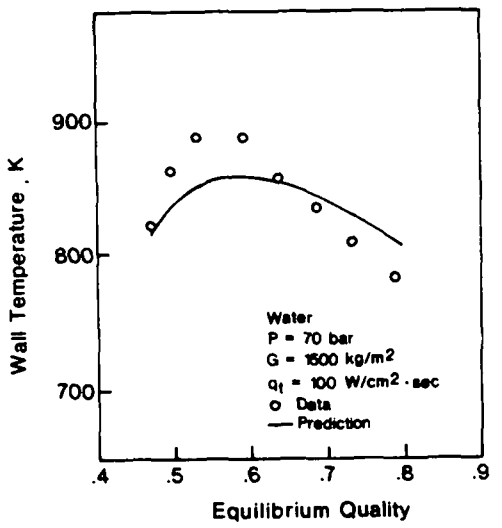

Fig. 13.

Figure 12. Comparison with Ling's water data (Ling *et al.* 1971).

Figure 13. Comparison with Ling's water data (Ling *et al.* 1971).

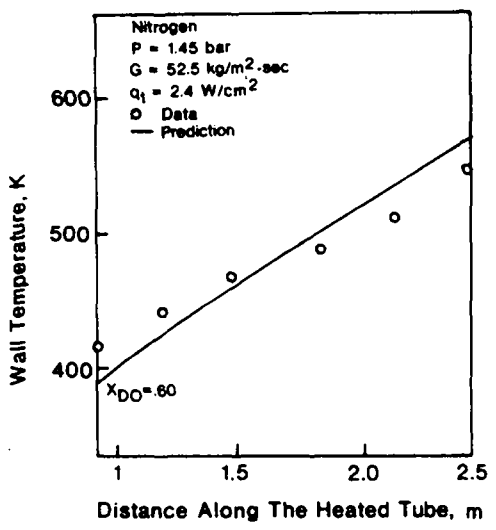

Fig. 14.

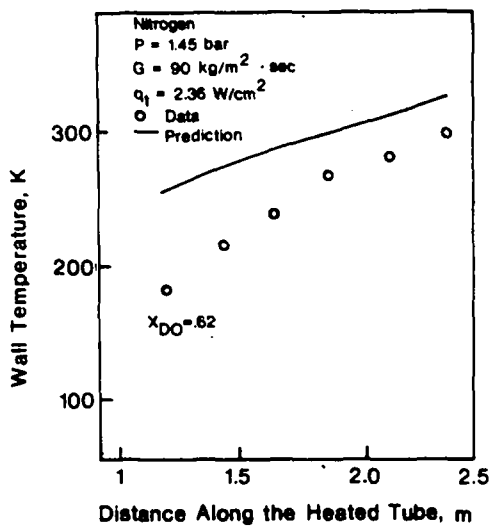

Fig. 15.

Figure 14. Comparison with Forslund's nitrogen data (Forslund & Rohsenow 1966).

Figure 15. Comparison with Forslund's nitrogen data (Forslund & Rohsenow 1966).

3.6 *Wall to droplet heat transfer*

This heat transfer mechanism is the least understood of the three mechanisms identified. However, the data of many workers indicates that the amount of heat transferred to an impinging droplet decays exponentially with increasing wall temperature (Holman & McGinnis 1969, Pederson 1967, Cumo & Farello 1972, Cumo *et al.* 1972, Wachters 1966, and Gaugler 1966). This decay has been estimated (Ganić & Rohsenow 1976) as:

$$\exp\left[1-\left(\frac{T_w}{T_s}\right)^2\right]. \qquad [24]$$

Holman & McGinnis (1969) concluded that a peak heat flux exists when a liquid droplet impinges on a hot surface. Their experiments with water, acetone, alcohol and some of the freons indicated that maximum heat flux occurs for temperature excesses of about 300°R. Their

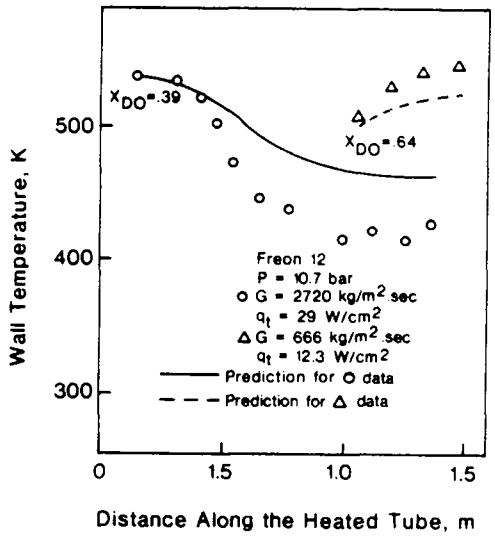

Figure 16. Comparison with Groeneveld's freon 12 data (Groeneveld 1972).

correlation, which seems to indicate the correct functional relationship between the parameters is:

$$\frac{Q_{max}}{\rho_L^{-3}\bar{D}_{10}H'_{LG}} = 1.83\times 10^{-3}\left(\frac{\rho_L^2 V_0^2 \bar{D}_{10}}{\rho_{vL}\sigma}\right)^{0.341} \quad [25]$$

where

$$H'_{LG} = H_{LG} + C_{pv}(T_w - T_v). \quad [26]$$

The maximum amount of heat to be transferred to droplet evaporating on the wall is given by:

$$Q_{max} = \frac{\pi}{6}\bar{D}_{10}^3\rho_L H'_{LG}. \quad [27]$$

Combining [24], [25], and [27] leads to the following expression for the efficiency of evaporation of an impinging liquid droplet:

$$\epsilon = 8.44\cdot 10^{-4}\left(\frac{\rho_L^2 V_0^2 \bar{D}_{10}}{\rho_{vL}\sigma}\right)^{0.341}\cdot \exp\left[1-\left(\frac{T_w}{T_s}\right)^2\right] \quad [28]$$

The total heat transfer from the wall to all impinging droplets can now be calculated using the relation by Ganić & Rohsenow (1976) as:

$$q_{wd} = V_0(1-\alpha)\rho_L H'_{LG} f_c \epsilon. \quad [29]$$

The droplet deposition velocity V_0 in dispersed flow is proportional to U^* and as indicated by Ganić & Mastanaiah (1981) is $\simeq 0.17U^*$ for a wide range of Re and droplet sizes. The turbulene deposition of droplets from dispersed flow onto the smooth wall of a tube has been extensively studied by Ganić & Mastanaiah (1981) where it was shown that V_0 depends on Re and the dimensionless relaxation time τ^+ ($= D^2\rho_G\rho_L U_*^2/18V_G^2$). Equation [18] in Ganić & Mastanaiah (1981) gives values of V_0 for a wider range of Re and τ^+ than those covered in this study.

The wall to drop heat transfer in dispersed flow, given by [29] depends on wall temperature

(via ϵ and f_c), droplet size distribution (also via ϵ and f_c), deposition velocity V_0 and the properties of the fluid. As mentioned by Ganić & Rohsenow (1976) oxide films, crud and wall micro-roughness can also affect wall-to-droplet heat transfer.

The expression of Hynek *et al.* (1969) for wall-to-drop heat transfer is quite different than [29]. It is based on evaporation of sessile droplets on a horizontal heated surface and includes two correlating constants K_1 and K_2 which are different for different fluids. It is possible that these correlating constants were needed since the droplet size distribution and deposition onto the heated wall were not considered.

3.7 *Wall temperature*

Based on the above, the wall temperature in the post dryout region can now be calculated as follows:

(a) Quantities assumed to be known at the dryout location are: q_t, G, X_{DO}, d, P and fluid properties as a function of temperature. The fluid properties are given by Plummer *et al.* (1974).

(b) The iteration technique of Hynek *et al.* (1969) modified by the inclusion of [14], is used to determine D_*, D_{32}, V_L and V_G. Thus the structure of the flow at the dryout location is completely defined.

(c) Assuming that the radiation heat transfer is negligible as cited by Plummer *et al.* (1974) the wall temperature at the dryout location (and each succeeding location), can be determined from the following heat balance:

$$q_t = q_{wv} + q_{wd} \qquad [30]$$

where

$$q_{wv} = h_{wv}(T_w - T_v) \qquad [31]$$

resulting in:

$$T_w = \frac{q_t - q_{wd}}{h_{wv}} + T_v \qquad [32]$$

where q_t is an input; h_{wv} is given by [23]; T_V is the local vapor temperature, which is equal to T_s at the dryout location; q_{wd} is given by [29].

Properties are evaluated at the local vapor temperature which is assumed to be the saturation temperature at the dryout location.

(d) Using the gradients presented earlier along with step size dZ the current values of V_v, V_L, D, X_a, X_e and T_v can be used to calculate the new values of V_L, D, X_a, X_e and T_v. The new value of the vapor velocity V_v, ic calculated from the continuity equation:

$$V_v = \frac{GX_a}{\rho_v} \Big/ \left(1 - \frac{G(1-X_a)}{\rho_L V_L}\right). \qquad [33]$$

The wall temperature T_w is then calculated using the heat balance in [32]. The wall to droplet component q_{wd} is calculated by determining the cutoff diameter, average impact diameter, effectiveness of evaporation and deposition factor. A variable step size in the flow direction is used to maintain accuracy near the dryout location while avoiding unnecessary calculations downstream where the gradients are relatively low. The following step sizes in feet have been

chosen:

$$\begin{aligned} dZ &= 0.0125 \text{ ft. } (3.81 \times 10^{-3} \text{ m}), && n < 20 \\ dZ &= 0.0250 \text{ ft. } (7.62 \times 10^{-3} \text{ m}), && 20 \leq n < 40 \\ dZ &= 0.0500 \text{ ft. } (1.524 \times 10^{-2} \text{ m}), && 40 \leq n < 60 \\ dZ &= 0.1000 \text{ ft. } (3.048 \times 10^{-2} \text{ m}), && n \geq 60 \end{aligned} \quad [34]$$

where n is the number of increments downstream.

4. COMPARISON WITH EXPERIMENTAL DATA

The model has been used to predict the experimental wall temperature profiles of several authors (Bennett *et al.* 1967, Forslund & Rohsenow 1966, Groenveld 1972, Era *et al.* 1966, Janssen & Kervinen 1975, Ling *et al.* 1971) for three different test fluids at various heat and mass fluxes. It should be noted that sizeable differences exist between the wall temperature profiles of different authors performing experiments under nearly identical conditions. Deviations on the order of fifteen percent are not uncommon. This implies that no single model will be able to accurately predict all of the data. However, various sets of data agree within reasonable limits, allowing trends to be identified and conclusions to be drawn.

4.1 *Water data*

The extensive experimental results of Bennett *et al.* (1967) were used as the primary data base for comparison with the model. The profiles chosen range from moderate to high void dryout.

The predicted profiles are shown as solid lines in figures 1–8. Examination of these results indicates no apparent dependence on heat or mass flux. However, the model does appear to agree more closely as the dryout quality increases. The reason for this is two-fold. First, the higher the dryout quality, the more likely the flow regime will be one of truly dispersed flow, on which the entire development of section 2 is based. At low dryout qualities the flow regime may be more of an inverse annular flow. In this case the modeling of the flow as dispersed, and hence the heat transfer calculations would be in error. This is most evident in figure 5, which while reasonably predicting the magnitude of the wall temperature, does a poor job of predicting the slope. Second, as the dryout quality increases the fraction of the flow that is in the liquid phase decreases. It is the liquid phase, which is involved in free stream evaporation and deposition on the heated wall, that leads to the uncertainty in the heat transfer calculations. Thus, as the dryout quality increases, the situation approaches the vapor limit, which is accurately modelled by the single phase vapor correlation.

The importance of the dryout droplet size and resulting free steam evaporation rate on the predicted wall temperature profile can be seen in figure 8. This illustrates the two limiting cases of evaporation rate. First, the frozen droplet model shows the predicted wall temperature profile when no evaporation takes place. This limit is approached as the droplet size increases, lowering the ratio of surface area (for heat transfer) to volume (proportional to the mass). Under these conditions the vapor rapidly superheats and wall temperatures rise sharply. The other extreme, namely the equilibrium model assumes that the vapor remains at the saturation temperature while droplets spontaneously evaporate absorbing any excess heat. This is the small droplet limit, characterized by a high ratio of surface area to mass. Thus, to predict the correct slope of the temperature profile the droplet size chosen must be representative of the surface area to mass ratio of the entire distribution. It appears that the Sauter mean diameter D_{32}, as given by [4] and [9], is successful in doing this. Overall agreement with the temperature profiles of Bennett *et al.* (1967) appears to be good in both magnitude and slope.

The component of heat flux transferred directly from the wall to liquid droplets ranged from nearly zero to about 10% at the dryout location depending on the experimental conditions. This fraction decreased downstream as the liquid phase diminished. As dryout qualities increased, the wall to liquid heat transfer rates decreased. The deposition factor (the mass fraction of the liquid entering the boundary layer that strikes the heated wall) was very close to one in all cases. This was due to the fact that the average droplet diameter was of the same order of magnitude or larger than the thickness of the boundary layer at $y^+ = 30$, where the trajectory calculation is initiated. The dryout droplet sizes ranged from 100 to 300 μm, while the boundary layer thicknesses ranged from about 20 to 100 μm. The resulting deposition diameters were on the order of ten percent of the boundary layer thickness. The mass contained in droplets smaller than the cutoff diameter was negligible in mass compared to the rest of the distribution. The efficiency of evaporation varied considerably depending upon the conditions, particularly the wall temperature. Typically, the efficiency of evaporation was on the order of 10^{-3} near the dryout location, then inversely proportional to the wall temperature at downstream locations. While this number may seem quite low, it must be kept in mind that only dry collisions are involved. Despite the value of the efficiency of evaporation, considerable amounts of heat can be transferred to the liquid due to the high heat of vaporization and the relatively large amount of liquid mass striking the wall.

The liquid phase becomes more uniform at downstream locations as the characteristic droplet size is decreased through evaporation. This shifts the distribution in the direction of small droplets. This variation in the distribution, along with actual and equilibrium quality profiles for a typical run is shown in figure 9.

Wall temperature profiles from the water data of Era *et al.* (1966), Janssen *et al.* (1975) and Ling *et al.* (1971) were also compared with the model. The results of these predictions are shown in figures 10–13. Again, there appears to be good agreement in both the magnitude and slope of the wall temperature profile. This indicates that the accuracy of the model does not depend on the data base chosen for comparison. This is not surprising however, since none of the correlations used in the model were developed by or based on the data of any of the authors used for comparison.

4.2 *Nitrogen data*

Figures 14 and 15 illustrate the comparison of the model with the nitrogen data of Forslund & Rohsenow (1968). Two different mass flow rates at approximately the same heat flux were compared. The predicted profile in figure 14 is in excellent agreement with the experimental data in both slope and magnitude. Figure 15 shows very good agreement with the slope of the experimental profile, however it also shows an over-prediction of the magnitude of the wall temperature.

4.3 *Freon data*

The general trends of the model are confirmed upon comparison with the freon 12 data of Groeneveld (1972). The choice of one high and one low dryout quality profile was made. And, as illustrated in figure 16 the model is more accurate for the high quality profile. The deposition factor, efficiency of evaporation, and fraction of the wall heat flux transferred directly to droplets followed patterns similar to those for water.

5. DISCUSSION OF HEAT TRANSFER TO DROPLETS AT OR NEAR THE HEATED WALL

The direct wall-to-liquid heat transfer was closely examined in this study. This component of heat transfer as calculated by [29] ranged for all predictions in this study, from nearly zero to about ten percent at the dryout location, then decreased downstream as the liquid phase diminished and wall temperature increased. It might be possible to neglect this mode of heat

transfer and compensate by adjusting the size of the droplets evaporating in the free stream (i.e. by decreasing the size in this case) to increase the vapor component of heat transfer. This has been demonstrated by Saha *et al.* (1977) where the droplet size was shown to control the evaporation rate of the droplets in the vapor core thereby controlling the vapor superheat. Presently experimental data exists on droplet sizes and size distributions (Cumo *et al.* 1973, Tatterson *et al.* 1977, Assopardi *et al.* 1978, Nukiyama & Tanasawa 1939, Boll *et al.* 1974 and James 1976) and predictions of evaporation rates should be based on these data.

The following are basic characteristics of wall to droplet heat transfer in dispersed flow.

(a) *Droplet-wall contact.* If the deposition velocity V_0 is relatively high, droplets penetrate the boundary layer and impact on the hot wall. Trajectories of droplet motion inside the boundary layer are shown by Ganić & Rohsenow (1976), where the effect of different parameters on droplet motion is examined. Droplet-wall contact is registered for temperatures of about 870 K above the Leidenfrost temperature (Tevepaugh & Keshock (1979)). This contact produces local cooling of the surface. A contacting boundary temperature is immediately established which depends on the initial liquid and wall temperatures and on the nature of the liquid and wall. An approximation of the contact temperature has been made by Iloeje *et al.* (1975) and Ganić & Rohsenow (1976) as:

$$(T_c - T_L)/(T_w - T_c) = [(k\rho C_p)_w/(k\rho C_p)_L]^{1/2} \quad [35]$$

In this case $T_L \simeq T_s$ since droplets in the vapor stream are at close to the saturation temperature. If T_c is less than the temperature of limiting superheat of the liquid at the system pressure, heat will be initially transferred from the wall to the droplet via conduction to be succeeded finally by film boiling.

(b) *Droplet evaporation inside the thermal boundary layer.* During the deposition motion of the droplets inside the boundary layer intensive evaporation takes place, since vapor superheat is much higher than inside the core.

The superheat inside the boundary layer is decreased due to rapid vapor generation giving rise to an increase in the convective heat transfer by the flowing vapor.

(c) *Destruction of the boundary layer.* At high impact velocities tiny droplets rebound from the hot wall with little cooling action. Large droplets are more likely to disintegrate upon impact. Many droplets of different sizes penetrate the boundary layer with some rebounding back through, thus destroying the laminar sublayer. Practically all resistance to heat transfer is concentrated within the boundary layer, and therefore the heat transfer to the vapor is greatly increased. In many applications the laminar sublayer is eliminated by using a rough surface. In the present work the liquid droplet motion inside the boundary layer serves as an artificial roughness.

It is clear that the above mechanisms (a)–(c) singly or in combination do not support neglecting q_{wd}. The fact that it is, at this stage of research, rather difficult to describe the above mechanisms with simplified relations for q_{wd} dictates the need for further research in this direction. The relation for q_{wd} used in this study, [29], does not include mechanisms (b) and (c) and therefore represents a lower limit of wall to droplet heat transfer.

In some cases where the heating along the flow channel is not uniform (i.e. $q_t = q_t(Z)$) serious errors may arise if q_{wd} is assumed negligible. For example, if q_t decreases downstream of the dryout location, the wall superheat will decrease. In that case, conditions downstream might exist where the wall superheat is less than the Leidenfrost superheat and rewetting of the surface will occur. In this situation the heat transfer to the liquid droplets can be one order of magnitude higher than the vapor component of heat transfer as shown by Ganić & Rohsenow (1976), Figures 8–17, in the range of $T_{CHF} < T < T_{Lf}$.

The post-dryout heat transfer model presented in this paper is also capable of handling wall heat fluxes that vary along the flow channel. A few examples of such cases are given by Moose & Ganić (1980).

6. SUMMARY AND CONCLUSIONS

Comparison of the model with experimental data found in the literature led to the following conclusions:

(a) The predicted wall temperature profiles are in good agreement in both slope and magnitude with the experimental profiles in the literature. Both water and freon 12 data indicate a dryout quality dependence of the model. Better agreement was found at higher qualities.

(b) The importance of the droplet size and size distribution was demonstrated through influence on the free stream evaporation and droplet deposition rates, and hence the wall temperature. The Sauter mean diameter defined in terms of a distribution and most probable droplet size appeared to be suitable for representing the liquid phase.

(c) The direct wall to liquid heat transfer mechanism was closely examined and combined mechanisms of wall to droplet heat transfer identified. The component of heat transfer from the wall to the liquid as predicted by [29] ranged from zero to ten percent of the total heat transfer near the dryout location, then decreased downstream as the liquid phase diminished and wall temperature increased.

Acknowledgement—This work was supported in part by the University of Illinois Research Board and NSF Grant ENG80-05681.

NOMENCLATURE

- A area, m^2
- C_D drag coefficient
- C_p specific heat at constant pressure, J/kg-K
- d tube diameter, m
- D droplet diameter, m or μm
- f_c deposition factor
- f_s smooth wall friction factor
- F arbitrary flow parameter
- g acceleration of gravity, m/s^2
- G mass flux, kg/m^2-s
- h heat transfer coefficient, W/m^2-K
- H specific enthalpy, J/kg
- H_{LG} specific latent heat of vaporization, J/kg
- k thermal conductivity, W/m-K
- m, n constants in [7] and [8]
- $n(D)$ drop size distribution function, m^{-1}
- P pressure, N/m^2
- Pr Prandtl number
- $P(D)$ probability function
- q heat flux, W/m^2
- Re Reynolds number
- T temperature, K
- U^* friction velocity, m/s
- V velocity, m/s
- We Weber number
- X quality
- y^+ dimensionless distance from the heated wall
- Z length or distance, m

Greek symbols

- α void fraction
- ϵ effectiveness of evaporation

Γ gamma function
μ dynamic viscosity, Pa-s
ρ density, kg/m^3
σ surface tension, N/m
τ^+ dimensionless relaxation time
μm microns (10^{-6} m)

Subscripts

a actual
c critical, contact
CHF critical heat flux
d droplet
D diameter
DO dryout
e equilibrium
L saturated liquid
G saturated vapor
0 impact
L liquid
L_f Leidenfrost
max maximum
mm mass median
m, n drop size indices
s saturated
t total
w wall
v vapor
vd vapor to drop
wd wall to drop
wv wall to vapor
* most probable
32 Sauter mean

REFERENCES

AZZOPARDI, B. J., FREEMAN, G. & WHALLEY, P. B. 1978 *Droplet sizes in annular two-phase flow.* Presented at the Winter Annual Meeting of the ASME, sponsored by the Heat Transfer Division, San Francisco, Dec. 10–15.

BENNETT, A. W., HEWITT, G. F., KEARSEY, H. A. & KEEYS, R. K. F. 1967 Heat transfer to steam–water mixtures flowing in uniformly heated tubes in which the critical heat flux has been exceeded. *Report No. AERE-R* 5373. Harwell.

BOLL, R. H., FLAIS, L. R., MAURER, P. W. & THOMPSON, W. L. 1974 Mean droplet size in a full scale venturi scrubber via transmissometer. *J. Air Pollution Assoc.* **24**, 934–938.

CHEN, J. C. SUNDARAM, R. K. & OZKAYNAK, F. T. 1977 A phenomenological correlation for post-CHF heat transfer. *NUREG Report*-0327.

CUMO, M., FARELLO, G. E. FERRARI, G. & PALAZZI, G. 1973 On two-phase highly dispersed flow. *ASME Paper No.* 73-*HT*-13.

CUMO, M. & FARELLO, G. E. 1972 Heated wall-droplet interaction for two-phase flow heat transfer in liquid deficient region. *CNEN-RT/ING*(72)19, pp. 146–178.

CUMO, M., FARELLO, G. E. & FERRARI, G. 1972 Notes on droplet heat transfer. *CNEN-RT/ING*(72)19, pp. 180–202.

ERA, A. *et al.* 1966 Heat transfer data in the liquid deficient region for steam–water mixtures at 70 kg/cm^2 flowing in tubular and annual conduits. *CISE-R*-184, *Topical report No.* 11.

FORSLUND, R. P. & ROHSENOW, W. M. 1966 Thermal non-equilibrium in dispersed flow film boiling in a vertical tube. *MIT Report No.* 75312-44.

FORSLUND, R. P. & ROHSENOW, W. M. 1968 Dispersed flow film boiling. *ASME Paper No.* 68-*HT*-44.

GANIĆ, E. N. & ROHSENOW, W. M. 1979 On the mechanism of liquid droplet deposition in two-phase flow. *J. Heat Transfer*, **101**, 288–294. Also *ASME Paper No.* 76-*WA*/*HT*-18.

GANIĆ, E. N. & ROHSENOW, W. M. 1976 Dispersed flow heat transfer. *Int. J. Heat Mass Transfer* **20**, 855–866.

GANIĆ, E. N. & MASTANAIAH, K. 1981 Investigation of droplet deposition from a turbulent gas stream. *Int. J. Multiphase Flow* **7**, 401–422.

GAUGLER, R. E. 1966 An experimental study of spray cooling on high temperature surfaces. Ph.D. Thesis, Carnegie Institute of Technology.

GROENEVELD, D. C. 1972 The thermal behavior of a heated surface at and beyond dryout. *AECL*-4309.

HINZE, J. O. 1949 Forced deformation of viscous liquid globules. *Appl Scientific Res.* **A1**, 263.

HOLMAN, J. P. & MCGINNIS, F. K. 1969 Individual droplet heat transfer rates for splattering on hot surfaces. *Int. J. Heat Mass Transfer* **12**, 95–108.

HYNEK, S. J. ROHSENOW, W. M. & BERGLES, A. B. 1969 Forced convection dispersed flow film boiling. *MIT Heat Transfer Lab. Report No* DSR 70586-63.

ILOEJE, O. C., ROHSENOW, W. M. & GRIFFITH, P. 1975 Three step model of dispersed flow in post-CHF. *ASME Paper No.* 75-*WA*/*HT*-1.

ISSHIKI M. 1959 Theoretical and experimental study on atomization of a liquid droplet in a high speed gas stream. *Report No.* 35, Transportation Technical Research Institute, Tokyo, Japan.

JAMES, P. W. 1976 A note on the applicability of a simple model of atomization to entrainment in annular two-phase flow. *AERE-M*2828.

JANSSEN, E. & KERVINEN, J. A. 1975 Film boiling and rewetting. General Electric Co. *Report No. NEDO*-20975.

LAVERTY, W. F. & ROHSENOW, W. M. 1964 Film boiling of saturated liquid nitrogen flowing in a vertical tube. *J. Heat Transfer* **89**, 90–98.

LING, C. H. *et al.* 1971 Temperature distribution for the post burnout regime in a round tube. Royal Institute of Technology, Laboratory of Nuclear Engineering, *Report No.* KTH-NEL-16, Stockholm.

MAYINGER, F. & LANGNER, H. 1978 Post-dryout heat transfer. *Proc. 6th Int. Heat Transfer Conf.*, Vol. 6, pp. 181–198. Toronto, Canada.

MICHIYOSHI, I. & MAKINO, K. 1979 Heat transfer characteristics of evaporation of a liquid droplet on heated surfaces. *Int. J. Heat Mass Transfer* **21**, 605–613.

MCADAMS, W. H. 1954 *Heat Transmission*, 3rd Edn, McGraw-Hill, New York.

MOOSE, R. A. & GANIĆ, E. N. 1980 Calculation of the wall temperature in the post dryout heat transfer region. University of Illinois, Dept. of Energy Engineering *Report NO.* TR-E-80-2.

NELSON, R. A. 1980 Forced convection post-CHF heat transfer and quenching. *ASME Paper No.* 80-WA/HT-69.

NIJHAWAN, S. M., CHEN, J. C. & SUNDARAM, R. K. 1980 Parametric effects on vapor non-equilibrium in post-dryout heat transfer. *ASME Paper No.* 80-WA/HT-50.

NUKIYAMA, S. & TANASAWA, Y. 1939 An experiment on the atomization of liquid by means of air stream. *Reports* 1 and 4. *Trans. Japan Soc. Mech. Engrs.*, **4**(14); **5**(18).

PEDERSON, C. O. 1967 The dynamics and heat transfer characteristics of water droplets impinging upon a heated surface. Ph.D. Thesis. Carnegie Institute of Technology.

PLUMMER, D. N., ILOEJE, O. C., ROHSENOW, W. M., GRIFFITH, P. & GANIĆ, E. N. 1974 Post critical

heat transfer to flowing liquid in a vertical tube. MIT Heat Transfer Lab. *Report No.* 72718-91.

SAHA, P., SHIRALKAR, B. S. & DIX, G. E. 1977 A post dryout heat transfer model based on actual vapor generation rate in dispersed droplet regime. *ASME Paper No.* 77-HT-80.

SHAMPINE, L. F., GORDON, M. K. (and modified by GOLLAND, R.). 1976 Using ODE/STEP, INTRP to solve ordinary differential equations. UICCAPP Library, University of Illinois Computer Center, Chicago, Illinois.

STYRIKOVICH, M. A., LEONTIEV, A. I., POLONSKY, V. S. & MALASHKIN, I. I. 1977 Investigation of post-dryout heat transfer in smooth and rough steam generating tubes. *Heat transfer—Soviet Res.* **9**, 123–131.

STYRIKOVICH, M. A., LEONTIEV, A. I., POLONSKY, V. S. & MALASHKIN, I. I. 1980 Analytical study of heat transfer in the post dryout region in smooth and rough vaporation channels. *Int. J. Heat Mass Transfer* **23**, 1045–1053.

TATTERSON, D. F., DALLMAN, J. C. & HANRATTY, T. J. 1977 Droplet sizes in annular gas liquid flows. *AIChE J.* **23**, 68–76.

TEVEPAUGH, J. A. & KESHOCK, E. G. 1979 Influence of artificial surface on film boiling heat transfer. *The 18th Nat. Heat Transfer Conf.*, San Diego, California.

WACHTERS, L. H. J. & WESTERLING, N. A. J. 1966 The heat transfer from a hot wall to impinging water droplets in the spheroidal state. *Chem. Engng Sci.* **21**, 1047–1056.

YARKHO, S. A., FILIN, N. V., IN'KOV, A. P., STAY'YEV, A. A. & UTKIN, V. N. 1977 Heat transfer, fluid dynamics and thermal inequilibrium in dispersed flow film boiling of hydrogen, nitrogen and argon in vapor generators. *Heat Transfer—Soviet Res.* **9**, No. 2.

YAO, S. & RANE, A. 1980 Numerical study of turbulent droplet flow heat transfer. *ASME Paper No.* 80-WA/HT-48.